Effects of Mechanical Vibration and Wall Thickness on Microstructure and Mechanical Properties of AZ91D Magnesium Alloy Processed by Expendable Pattern Shell Casting

WENMING JIANG, ZITIAN FAN, XU CHEN, BENJING WANG, and HEBAO WU

Mechanical vibration was introduced into the solidification process of AZ91D magnesium alloy during the expendable pattern shell casting process, and the combined effects of mechanical vibration and wall thickness on the microstructure and mechanical properties were investigated. The results indicate that with the increase of wall thickness, the morphologies in α-Mg phase and β-$Mg_{17}Al_{12}$ phase of the samples obtained without vibration evolved from a fine dendrite to a coarse dendrite and from a fine continuous network structure to a coarse continuous network structure, respectively, and the mechanical properties and density of AZ91D alloy continuously decreased. With the application of mechanical vibration, the coarser dendrites transformed into fine equiaxed grains, and the previous coarse continuous network structure of the β-$Mg_{17}Al_{12}$ phase was changed to a discontinuous granular morphology. Meanwhile, the mechanical properties and density of AZ91D alloy greatly increased. The effect of mechanical vibration on the microstructure and mechanical properties increased with increasing vibration frequency and wall thickness. The fractographs of the tensile samples show a change in fracture surface from brittle to that of a tough fracture with the addition of vibration.

DOI: 10.1007/s11661-015-2746-2

I. INTRODUCTION

CURRENTLY, complicated and thin-walled magnesium alloy precision castings are widely used in the aerospace and automotive industries owing to their many advantages including low density, high specific strength, electromagnetic shielding capacity, good machinability as well as excellent castability.[1–4] The expendable pattern shell casting process is a precision casting technology and suitable for manufacturing complicated and thin-walled magnesium and aluminum alloys precision castings with a high quality,[5–7] which was first proposed by Ashton *et al.*[8] This precision casting process adopts the foam pattern preparation of the lost foam casting (LFC) and thin shell precision fabrication of the investment casting. First, the foam pattern based on the part shape is prepared as a prototype, and then the thin shell is fabricated using the shell fabrication technology of investment casting outside the foam prototype. Subsequently, the foam prototype is removed and the thin shell is roasted. Lastly, the filling and solidification of the molten metal is completed under vacuum after boxing and modeling.[9]

The expendable pattern shell casting process has some advantages, such as flexible design and low cost of foam pattern, high precision of investment casting as well as good forming ability. The porosity and slag inclusion defects in the LFC process because of the decomposition of the foam pattern during casting process can be fully avoided because the foam pattern has been removed before pouring. On the other hand, the filling ability and feeding capacity of the molten metal can also be improved because the filling and solidification of the molten metal is carried out under vacuum. Unfortunately, the microstructures of magnesium alloy precision castings obtained using the expendable pattern shell casting process show a coarse dendritic structure with an inhomogeneous distribution, and the β-$Mg_{17}Al_{12}$ phase forms a coarse continuous network structure, especially the castings with a larger wall thickness, leading to a sharp decrease of mechanical properties.

In general, the refinement of microstructure has many methods, such as chemical elements modification,[10,11] electromagnetic vibration,[12,13] ultrasonic vibration,[14,15] combination of electromagnetic and ultrasonic fields,[16] and mechanical vibration.[17,18] The mechanical vibration has the potential to be a simple, economic, and effective method to refine microstructure and improve mechanical properties,[19] which was first applied on the steel by Chernov.[20]

WENMING JIANG, Associate Professor, is with the State Key Lab of Materials Processing and Die and Mould Technology, Huazhong University of Science and Technology, Wuhan 430074, P.R. China, and also with the School of Mechanical & Electrical Engineering, Wuhan Institute of Technology. Contact e-mail: jwenming@163.com ZITIAN FAN, Professor, is with the State Key Lab of Materials Processing and Die and Mould Technology, Huazhong University of Science and Technology. XU CHEN and BENJING WANG, Students, and HEBAO WU, Professor, are with the School of Mechanical & Electrical Engineering, Wuhan Institute of Technology.

Manuscript submitted September 9, 2014.
Article published online 22 January 2015

In this present work, a simple and economic mechanical vibration method was first introduced into the solidification process of the AZ91D magnesium alloy during the expendable pattern shell casting process aiming at the improvement of microstructure and mechanical properties. It should be noted that the vibration equipment for compacting loose sand can be used as a vibration source for the casting. Meanwhile, the effect of wall thickness on the microstructure and mechanical properties of AZ91D magnesium alloy was also comprehensively considered. The main objective of the present work is to investigate the combined effects of mechanical vibration and wall thickness on the microstructure and mechanical properties of AZ91D magnesium alloy obtained by the expendable pattern shell casting process.

II. EXPERIMENTAL PROCEDURES

The foam pattern samples with a step shape were first prepared using the foaming molding process, and the wall thicknesses of the foam pattern samples are 10, 20, 30, and 40 mm, respectively, as shown in Figure 1. Secondly, the ceramic shell was fabricated with coating the foam pattern using the ceramic slurry and refractory to form the stucco on the coated foam pattern. Subsequently, the foam pattern and shell were roasted to harden the shell and remove the foam. The shell was then placed in a sand flask, the sand flask was filled with unbonded loose sand, and the loose sand was compacted using a vibration table, and finally the sand flask was covered with a plastic film. The ceramic mold cavity is now ready for pouring.

Commercial AZ91D magnesium alloy was used in this study, and its chemical composition is shown in Table I. The stainless steel crucible was first preheated at 573 K (300 °C) in an electrical resistance furnace, and the preheated AZ91D magnesium alloy ingots were then placed inside the stainless steel crucible to melt under the CO_2-0.5 pct SF_6 protective gas mixture. When the temperature of the molten metal reached 1003 K (730 °C), the slag of the molten metal was skimmed, and the molten metal was then poured into the ceramic mold cavity after started the vacuum pump and vibration table. First, the different vibration frequencies were investigated for 0, 35, 50, 100, and 120 Hz, respectively, and castings were made under different vibration frequencies with constant temperature, pouring rate, and metal composition. Subsequently, the comparative experiments between with and without vibration methods were processed under different wall thicknesses, and the vibration frequency was 100 Hz for the vibration method. Figure 2 presents a schematic illustration of experimental apparatus for the mechanical vibration during the expendable pattern shell casting process.

Metallographic samples were polished and then etched with a 4 pct Nital solution. Microstructures of the samples were observed using a Me F-3 metallographic microscope or a Quanta 400 scanning electron microscope (SEM; FEI Corporation, Hillsboro, OR), and the microstructural features of the samples were also identified using an energy dispersive spectrophotometric (EDS) analysis. The average length of β-$Mg_{17}Al_{12}$ particles and average width of β-$Mg_{17}Al_{12}$ particles were measured by using the Image Tool metallographic analysis software. The aspect ratio of β-$Mg_{17}Al_{12}$ particles was taken as the ratio of the average length of β-$Mg_{17}Al_{12}$ particles to the average width of β-$Mg_{17}Al_{12}$ particles. The measurement was done on 50 different areas of each microstructure in order to minimize the errors. The grain size (D) and shape factor (F) of the α-Mg primary phase were defined as follows:[21,22]

$$D = 2\sqrt{\frac{A}{\pi}} \qquad [1]$$

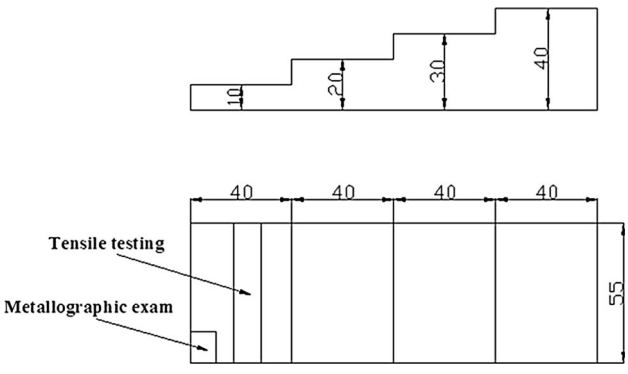

Fig. 1—Schematic for step sample (unit: mm).

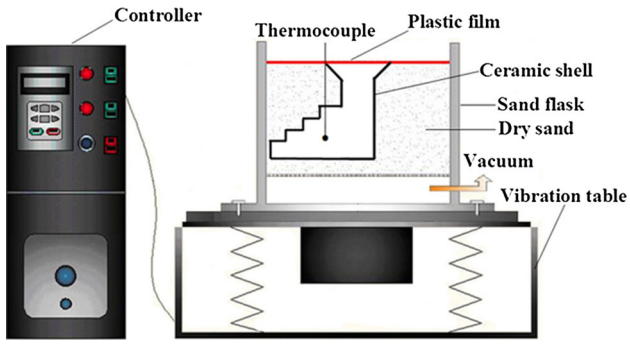

Fig. 2—Schematic illustration of experimental apparatus for the mechanical vibration during the expendable pattern shell casting process.

Table I. The Nominal Chemical Composition of Experimental Alloy (Weight Percent)

Element	Al	Zn	Mn	Si	Fe	Cu	Ni	Mg
Wt pct	8.96	0.8	0.28	0.07	0.039	0.024	0.001	balance

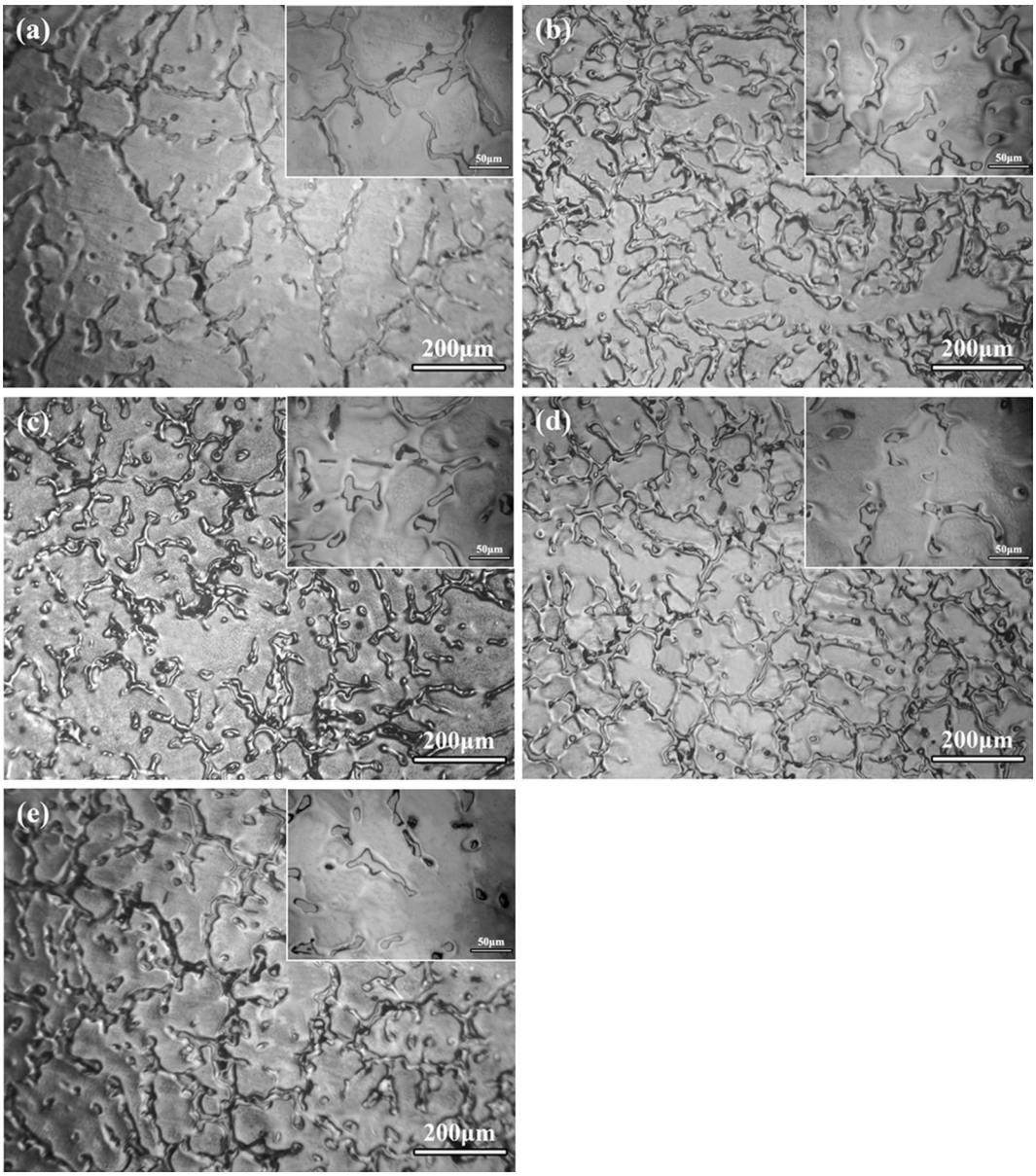

Fig. 3—Optical microstructures of the as-cast AZ91D magnesium alloy obtained by different vibration frequencies: (*a*) 0 Hz, (*b*) 35 Hz, (*c*) 50 Hz, (*d*) 100 Hz, and (*e*) 120 Hz.

$$F = \frac{4\pi A}{P^2}, \qquad [2]$$

where A and P are the average area and average perimeter of α-Mg primary grain, respectively, which were measured using the Image Tool software. F value varies from 0 to 1, and the sectional shape of α-Mg grain approaches to a circle when it is close to 1.

Densities of the AZ91D alloy castings were measured by using Archimedes' method. Tensile tests were performed using a ZwickZ100 universal testing machine at room temperature with a crosshead speed of 0.5 mm/min. The tensile test samples with a gage length of 13 mm and a rectangular (1.6 × 3 mm) cross section were cut from the sampling positions as shown in Figure 1. The hardness measurements were carried out using a HBE-3000A hardness tester, and the load and holding time were 250 kg and 15 seconds, respectively. The fractured surfaces of the tensile samples were observed and analyzed using the SEM and EDS methods.

III. RESULTS AND DISCUSSION

A. *Effect of Vibration Frequency on Microstructure of AZ91D Magnesium Alloy*

Figure 3 depicts the optical microstructures of the as-cast AZ91D magnesium alloy obtained by different vibration frequencies during the expendable pattern shell casting process. Meanwhile, the optical microstructures of the eutectic zone have been shown in order to demonstrate a substantial microstructure difference in

the morphology, size, and distribution of β-$Mg_{17}Al_{12}$ phase. It can be seen from Figure 3 that the microstructures of the as-cast AZ91D magnesium alloy obtained by the expendable pattern shell casting process mainly consist of α-Mg primary phase and β-$Mg_{17}Al_{12}$ phase, and the white matrix phase is α-Mg, and the gray phase along grain boundaries is β-$Mg_{17}Al_{12}$. As can also be seen, a typical coarse dendrite microstructure is observed from the microstructure of the AZ91D magnesium alloy without vibration (0 Hz), and the β-$Mg_{17}Al_{12}$ phase shows a coarse continuous network structure, as shown in Figure 3(a). With the application of mechanical vibration, the microstructure of the AZ91D magnesium alloy is significantly improved, and the grain size of α-Mg primary phase gradually decreases with the increase of vibration frequency, and the β-$Mg_{17}Al_{12}$ phase exhibits a discontinuous granular structure. With a vibration frequency of 100 Hz, the microstructure mainly consists of fine equiaxed grains with a uniform distribution, as shown in Figure 3(d). With further increasing vibration frequency, grains begin to coarsen.

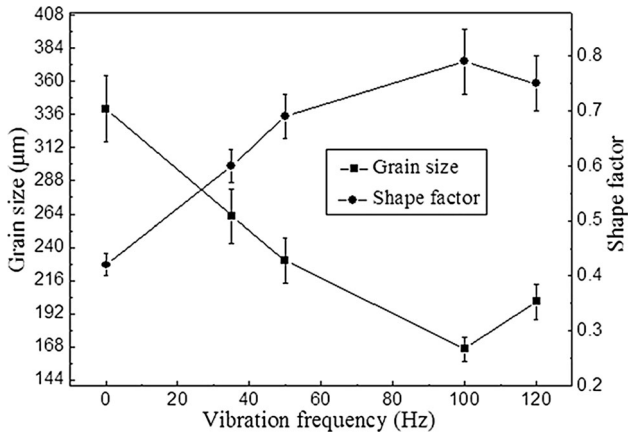

Fig. 4—Effects of vibration frequency on grain size and shape factor of the α-Mg primary phase.

Figure 4 presents the quantitative metallography assessment of the microstructural features of α-Mg primary phase under different vibration frequencies. It is

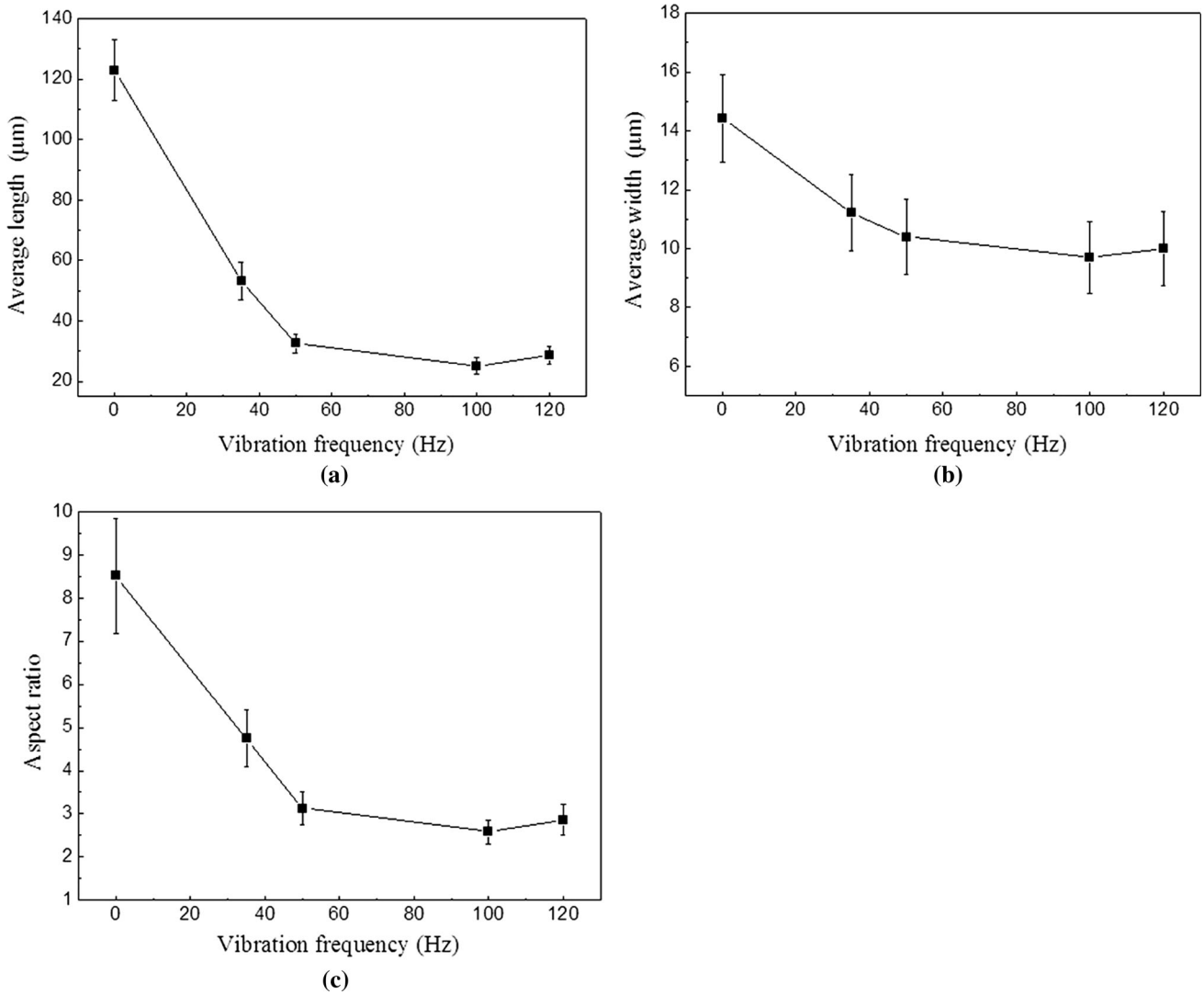

Fig. 5—Effects of vibration frequency on (*a*) average length, (*b*) average width, and (*c*) aspect ratio of $Mg_{17}Al_{12}$ particles.

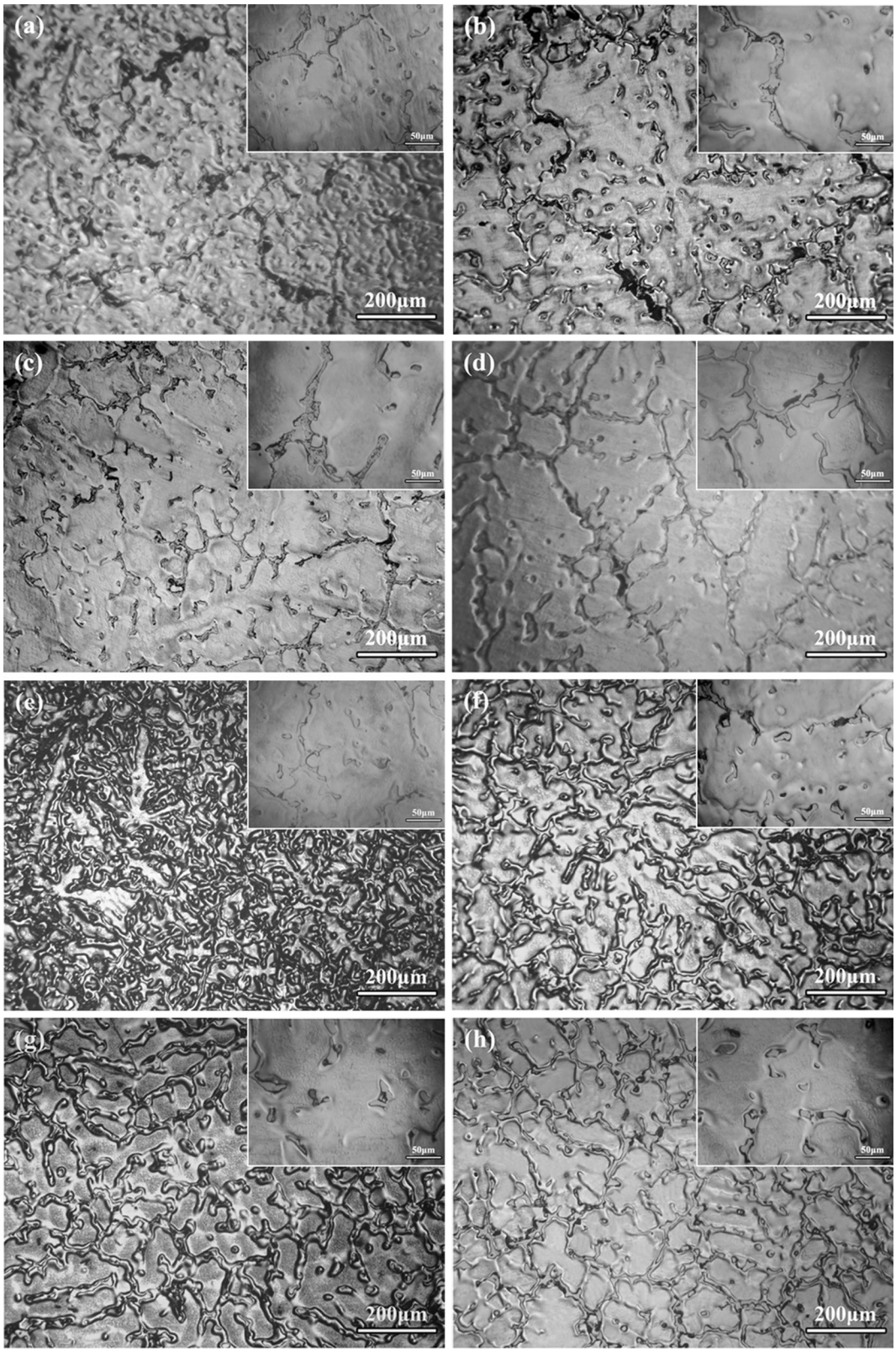

Fig. 6—Optical microstructures of the as-cast AZ91D magnesium alloy obtained from (*a*, *e*) 10 mm, (*b*, *f*) 20 mm, (*c*, *g*) 30 mm, (*d*, *h*) 40 mm, (a–d) without vibration and (e–h) with vibration (100 Hz).

evident that the mechanical vibration greatly decreases the grain size and increases the shape factor of α-Mg primary phase. With increasing vibration frequency, the grain size gradually decreases, and the shape factor continuously increases. When the vibration frequency is 100 Hz, the grain size decreases 51 pct and the shape factor increases 88 pct compared with that of the sample without vibration. Consequently, the mechanical vibration significantly improved the size and morphology of α-Mg primary phase.

Figure 5 shows the quantitative metallography assessments for the β-$Mg_{17}Al_{12}$ particles under different vibration frequencies. It is noted that the average length, width, as well as aspect ratio of the β-$Mg_{17}Al_{12}$ particles obtained with vibration significantly decreased compared to that of the sample without vibration. Moreover, the average length, width, and aspect ratio of the β-$Mg_{17}Al_{12}$ particles gradually decrease with increasing vibration frequency. With a vibration frequency of 100 Hz, the average length, width, and aspect ratio are 80, 33, and 70 pct lower than that of the sample without vibration, respectively.

B. *Combined Effect of Mechanical Vibration and Wall Thickness on Microstructure of AZ91D Magnesium Alloy*

Figure 6 shows the optical microstructures of the as-cast AZ91D magnesium alloy with different wall thicknesses obtained with and without vibration methods. In the microstructures obtained from the samples without vibration, it is evident that the typical dendrites of α-Mg primary phase are observed and show non-uniform distributions, as shown in Figures 6(a) through (d). Meanwhile, with increasing wall thickness, the α-Mg primary phase transforms from a fine dendrite to a coarser dendrite, and the β-$Mg_{17}Al_{12}$ phase forms a coarser continuous network structure. For comparison, in the microstructures obtained from the samples with vibration, it is obvious that the grain sizes of α-Mg primary phase are much finer than that of the samples without vibration under the same wall thickness, coarse dendrites have almost disappeared, microstructures mainly consist of equiaxed grains with an uniform distribution, and the β-$Mg_{17}Al_{12}$ phase shows a discontinuous granular structures, as shown in Figures 6(e) through (h). In particular, with the increase of wall thickness, the number of equiaxed grains gradually increases. With a wall thickness of 40 mm, many fine equiaxed grains can be observed, as shown in Figure 6(h).

Figures 7 and 8 present the quantitative metallography assessment of the microstructural features of α-Mg primary phase. For the samples without vibration, with the increase of wall thickness from 10 to 40 mm, there is a sharp increase in grain size from about 205 to 340 μm. Compared with the samples without vibration, the grain size of the samples with vibration significantly decreases, and the grain size is only about 166 μm with a wall thickness of 40 mm. With increasing wall thickness, the difference in the grain size between the samples with and without vibration is a substantial increase. Besides, it is noted from Figure 8 that the mechanical vibration greatly increases the spherical degree of α-Mg primary phase, particularly the samples with a larger wall thickness.

Figure 9 depicts the quantitative metallography assessments of the microstructural features of β-$Mg_{17}Al_{12}$ particles from the samples with different wall thicknesses obtained with and without vibration methods. It is noted that the average length, width as well as aspect ratio of β-$Mg_{17}Al_{12}$ particles from the samples without vibration increase continuously with increasing wall thickness. For comparison, the average length, width, and aspect ratio of β-$Mg_{17}Al_{12}$ particles from the samples with vibration are obviously smaller compared to that of the samples without vibration. The difference in the average length, width, and aspect ratio of β-$Mg_{17}Al_{12}$ particles between the samples obtained with and without vibration increases with an increase in wall thickness.

It is well known that the microstructure of alloy mainly depends on the nucleation stage and subsequent

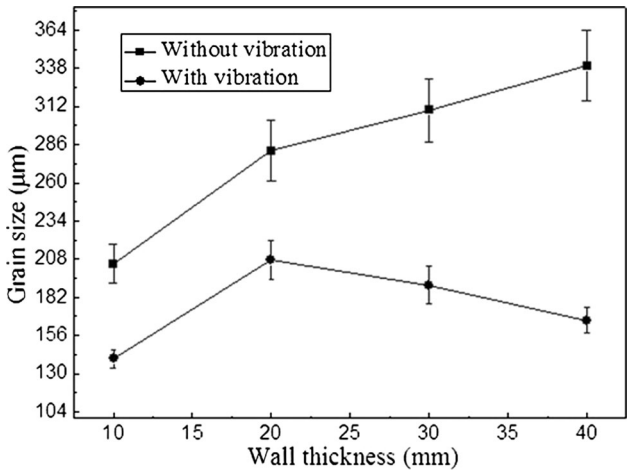

Fig. 7—Effect of mechanical vibration and wall thickness on grain size of the α-Mg primary phase.

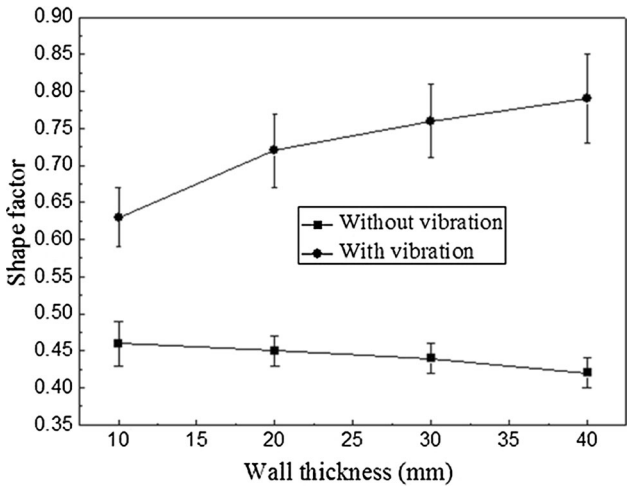

Fig. 8—Effect of mechanical vibration and wall thickness on shape factor of the α-Mg primary phase.

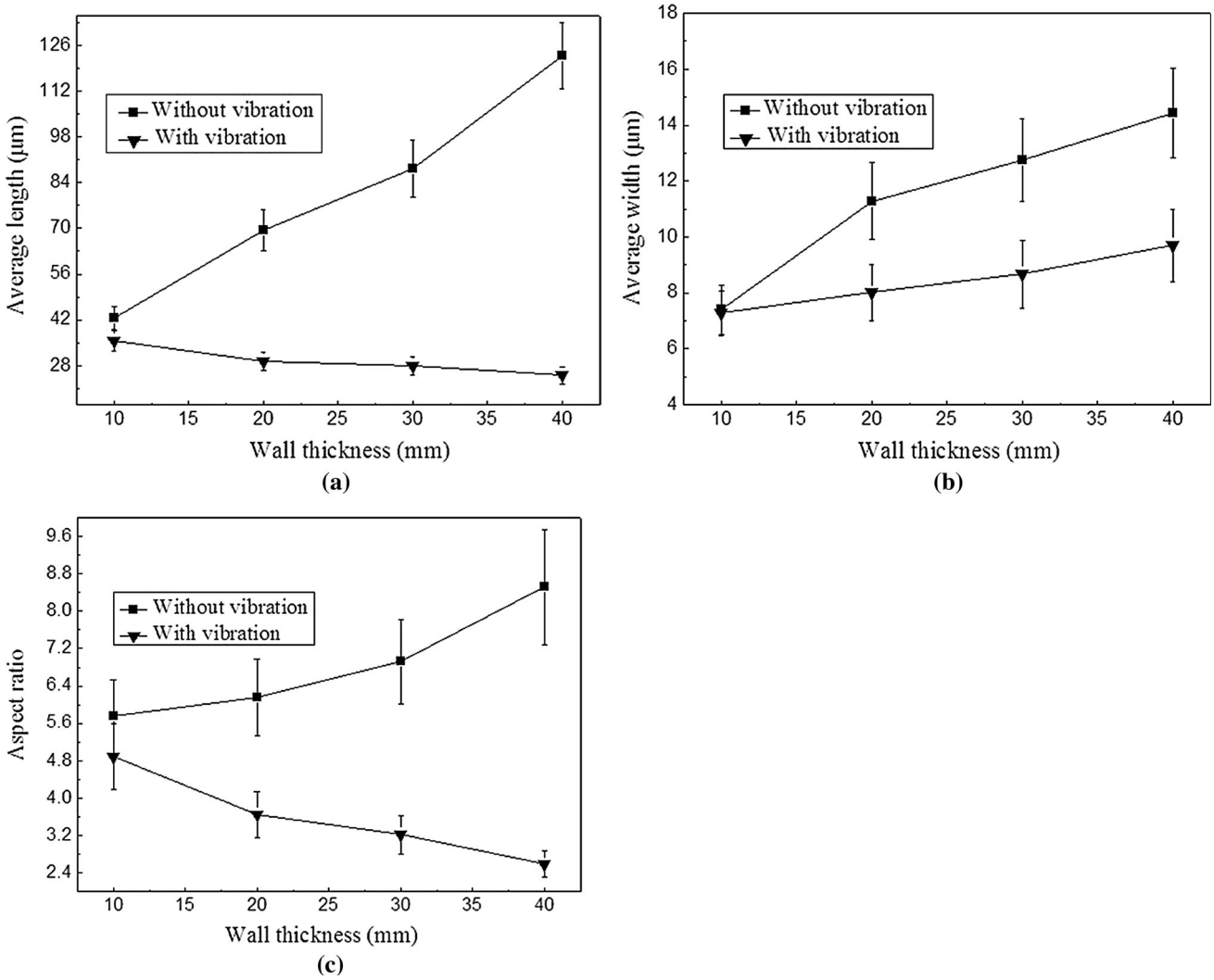

Fig. 9—Effects of mechanical vibration and wall thickness on (*a*) average length, (*b*) average width, and (*c*) aspect ratio of $Mg_{17}Al_{12}$ particles.

growth condition, and the sufficient nuclei are essential to the microstructural refinement. For the without vibration condition, with the increase of wall thickness, the cooling rate of the molten metal decreases, and the solidification time of the molten metal increases, and there is no sufficient nuclei to generate in the melt during the solidification process, which promotes a coarser microstructure.

With the application of mechanical vibration in the solidification process of the alloy, the significant refinement of final microstructure can be explained by the following mechanism. Generally, it has been noted that the vibration energy influences on the final microstructure mainly in two manners: creating periodic tension-pressure and forced convection in the molten alloy.[19,23] However, the periodic tension-pressure generated in the molten metal easily gives rise to the cavitation phenomena, especially the high frequency vibrations, like ultrasonic vibration, and it cannot be the main reason for the microstructural refinement in this work. Consequently, the forced convection in molten alloy may be mainly responsible for the microstructural refinement in this study. This can be explained by the fact that the vibration energy induces a forced convection in the molten metal. Moreover, flows induced by vibration

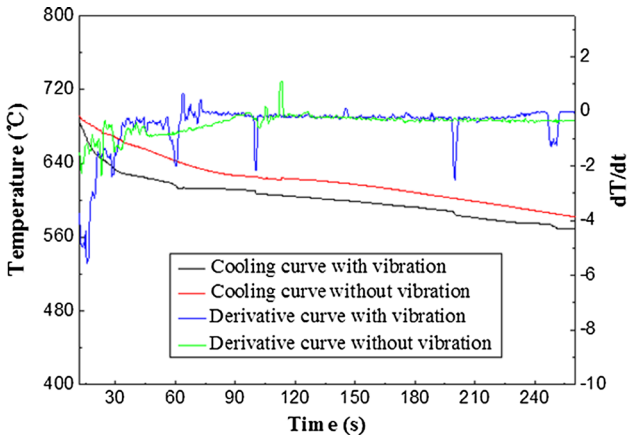

Fig. 10—Representative cooling curves of the molten metal recorded with and without vibration methods.

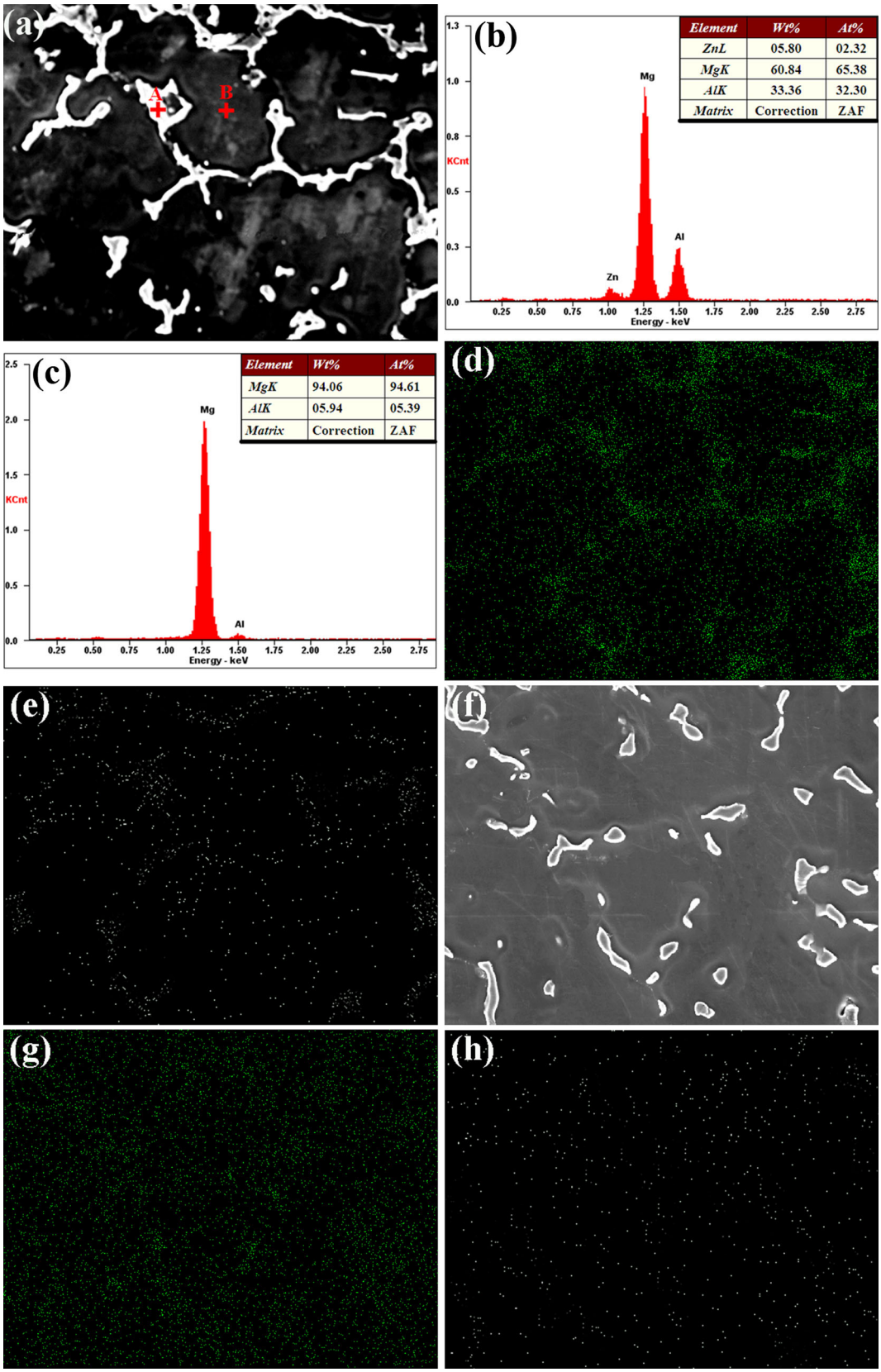

Fig. 11—SEM micrographs of (*a*) without vibration and (*f*) with vibration; (*b*) and (*c*) EDS corresponding to *A* and *B* of (a), respectively; EDS of (*d*) Al K and (*e*) Zn K of without vibration, (*g*) Al K and (*h*) Zn K of with vibration.

insert external forces on dendrite arms in flow direction.[24] The liquid metal begins to quickly solidify as it comes in contact with the cold mold wall. As a result, the initial solidified fine dendrites forming on the cold wall of the mold are easily broken off by the vibrating forces from the mechanical vibration. Meanwhile, the detached dendrite arms can be carried by the forced convection into the bulk melt, acting as new nuclei. With the further detachments of dendrite arms, the nucleation rate gradually increases, resulting in a significant refinement of the microstructure.

On the other hand, the final microstructure is determined not only by the nucleation, but also by the growth condition. The vibration also induces a high heat transfer inside the molten metal to the mold interface as result of the alternated movement of the molten metal, leading to a high solidification rate of the molten metal. Figure 10 compares the cooling rates of the molten metal obtained with and without vibration methods. It is evident that the cooling rate of the molten metal with vibration is faster than that of the molten metal without vibration, and it is in agreement with the previous studies.[25,26] It means that the faster cooling rate of the molten metal under the vibration condition gives rise to a larger undercooling and thereby stimulates more existing nuclei in the molten metal to start a spontaneous heterogeneous solidification, leading to the refinement of microstructure.

Moreover, the vibration treatment also enhances the mass transfer and diffusion processes of solidified alloy due to the strong forced convection. Figure 11 shows the SEM micrographs and EDS analysis obtained with and without vibration methods. Figures 11(b) and (c) point out β-$Mg_{17}Al_{12}$ phase and α-Mg primary phase, respectively, corresponding to A and B in Figure 11(a). Compared to Figures 11(a) and (f), it is clear that the vibration method significantly improves the morphology and distribution of β-$Mg_{17}Al_{12}$ phase, and it is consist with Figures 3 and 6. Meanwhile, it can also be seen that the composition distributions of Al and Zn elements from the sample without vibration are inhomogeneous, and they mainly enrich in the grain boundary, as shown in Figures 11(d) and (e). With the application of mechanical vibration, it is noted that the EDS of Al K and Zn K are obvious homogeneous than that of the sample without vibration, as shown in Figures 11(g) and (h). In this case, the growth of dendrite is limited and thereby generates many equiaxed grains, resulting in the further refinement of microstructure.

In addition, the larger wall thickness increases the solidification time of the molten metal. That means that the action time and effect of mechanical vibration on the molten metal are significantly improved and thereby increase the grain refinement degree.

C. *Combined Effect of Mechanical Vibration and Wall Thickness on Mechanical Properties of AZ91D Magnesium Alloy*

Figures 12 and 13 show the effect of mechanical vibration and wall thickness on mechanical properties of AZ91D magnesium alloy. As can be seen, for the

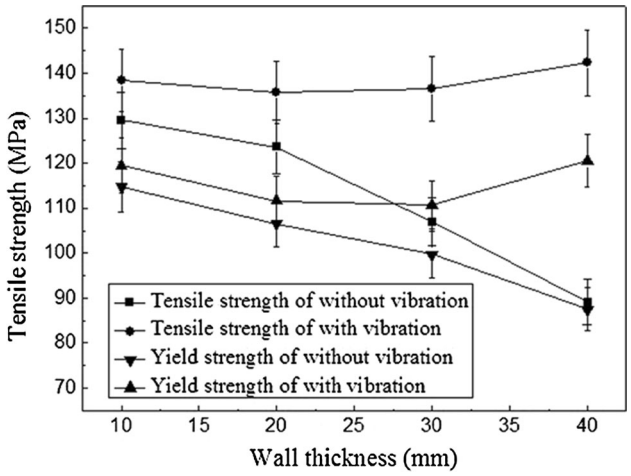

Fig. 12—Effect of mechanical vibration and wall thickness on tensile strength of AZ91D magnesium alloy.

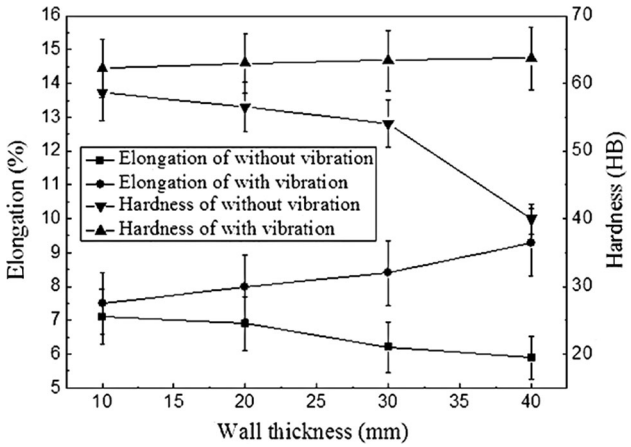

Fig. 13—Effects of mechanical vibration and wall thickness on elongation and hardness of AZ91D magnesium alloy.

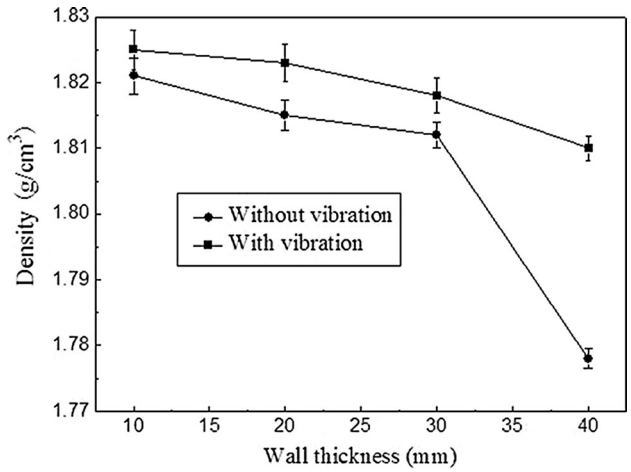

Fig. 14—Effect of mechanical vibration and wall thickness on density of AZ91D magnesium alloy.

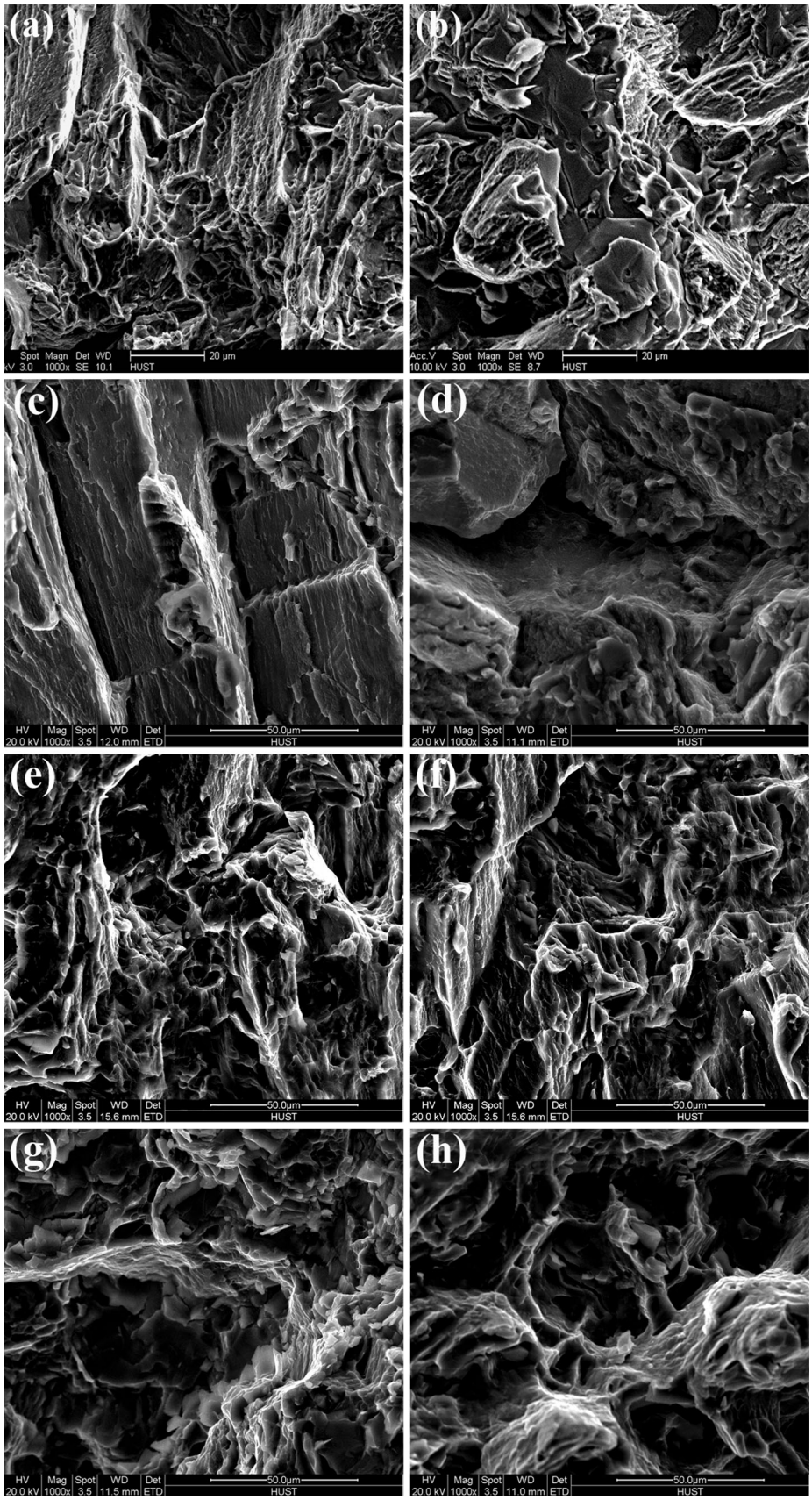

Fig. 15—SEM fractographs of AZ91D magnesium alloy tensile samples obtained from (*a*, *e*) 10 mm, (*b*, *f*) 20 mm, (*c*, *g*) 30 mm, (*d*, *h*) 40 mm, (a–d) without vibration and (e–h) with vibration (100 Hz).

samples without vibration, the mechanical properties including tensile strength, yield strength, elongation, and hardness gradually decrease with the increase of wall thickness. This can be explained by the fact that the larger wall thickness promotes a coarser microstructure. The size, morphology, and distribution of the α-Mg primary phase and β-$Mg_{17}Al_{12}$ phase have a great effect on the mechanical properties of AZ91D magnesium alloy.[27] According to the following Hall–Petch relationship[20,28]

$$\sigma_s = \sigma_0 + k \cdot d^{-1/2}, \quad [3]$$

where σ_s is the yield strength, σ_0 is the lattice friction stress from the dislocation motion, k is the enhancement coefficient, and d is the average grain size. Because σ_0 and k mainly depend on the composition of the alloy, d has a decisive effect on the yield strength of the alloy, especially the magnesium alloy with a close-packed hexagonal structure.[29] Moreover, the β-$Mg_{17}Al_{12}$ phase is a hard and fragile metallic compound, and the large-sized β-$Mg_{17}Al_{12}$ particles are always harmful to the mechanical properties.[30] As a result, a fine microstructure will greatly increase the mechanical properties of the magnesium alloy.

After processing with mechanical vibration, the mechanical properties show a significant improvement compared to those processed without vibration, especially the larger wall thickness. With a wall thickness of 40 mm, the tensile strength, yield strength, elongation as well as hardness of the sample with vibration are, respectively, 60, 38, 58, and 59 pct higher than that of the sample without vibration. Meanwhile, the difference in mechanical properties between the samples obtained with and without vibration increases with an increase in wall thickness. The advantages of size, morphology, and distribution of α-Mg primary phase and β-$Mg_{17}Al_{12}$ phase are responsible for the improvement of mechanical properties of the AZ91D magnesium alloy with vibration compared with that of the alloy without vibration.

Besides, it can also be observed from Figure 14 that the density of the AZ91D magnesium alloy with vibration is higher than that of the alloy without vibration, especially the larger wall thickness, and it can be explained by the fact that the mechanical vibration promotes the filling ability and feeding capacity of the molten metal,[23] resulting in the improvement of compactness of the AZ91D magnesium alloy. As a result, the mechanical properties of AZ91D magnesium alloy with vibration are further increased compared with that of the alloy without vibration.

D. *Combined Effect of Mechanical Vibration and Wall Thickness on Fractography of AZ91D Magnesium Alloy*

Figure 15 shows the SEM fractographs of AZ91D magnesium alloy tensile samples with different wall thicknesses obtained with and without vibration methods. It is clear that the SEM fractographs of AZ91D magnesium alloy tensile samples produced without vibration method reveal typical brittle fracture natures, and the obvious cleavage planes can be observed, as shown in Figures 15(a) through (d). For the samples without vibration, the hard and fragile β-$Mg_{17}Al_{12}$ phase with a large-sized net-like structure will generate a large stress concentration, and it is easy to crack. As a result, the crack propagation path for the sample produced without vibration goes through the secondarily solidified structures of β-$Mg_{17}Al_{12}$ phase, as shown in Figure 16. Finally, it reveals a brittle fracture nature. Moreover, the porosity defect can also be observed from the SEM fractograph of the AZ91D magnesium alloy tensile sample without vibration, as shown in Figure 15(d). Meanwhile, the shrinkage porosity defects are also observed from the SEM fractograph obtained without vibration, as shown in Figure 17. As a consequence, the fracture path may preferentially go through the porosity defects in the case of the existence of excessive porosity defects, resulting in poorer mechanical properties.

For comparison, the SEM fractographs of the AZ91D magnesium alloy tensile samples with vibration exhibit morphologies of dimple fracture, particularly the larger wall thickness, as shown in Figures 15(g) and (h). It should be noted that the AZ91D magnesium alloy gives rise to a large plastic deformation. Because the samples with vibration have a finer α-Mg primary phase, dispersively distributed β-$Mg_{17}Al_{12}$ particles as well as

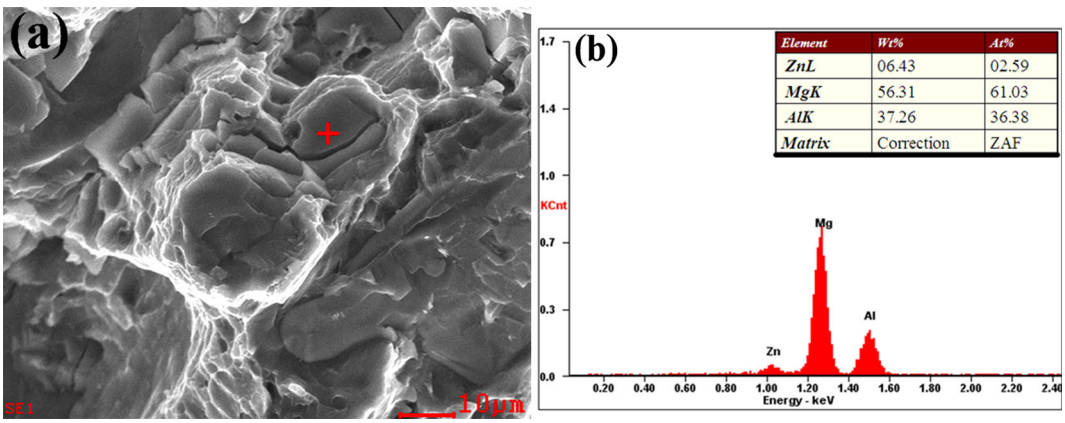

Fig. 16—SEM fractographs of the tensile sample without vibration: (*a*) Fractograph and (*b*) EDS.

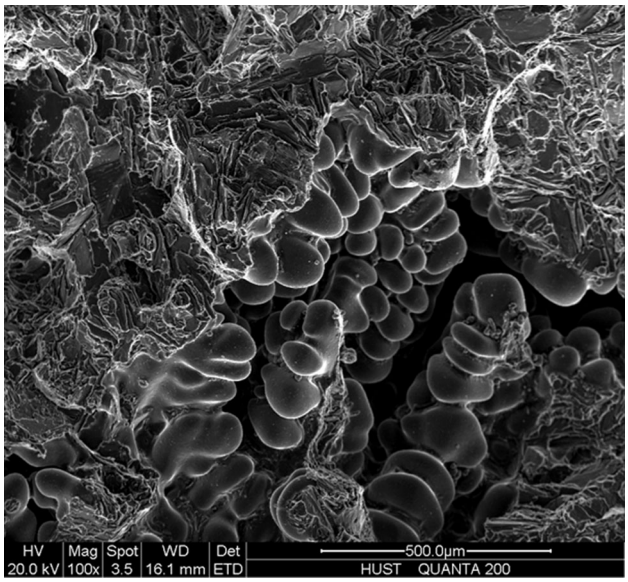

Fig. 17—Shrinkage defects of the tensile sample without vibration.

a higher compactness, the smaller stress concentration occurs, and the crack propagation gradually changes into completely across the α-Mg primary phase.[31] As a result, the fracture surface is dominated by some dimples, and it finally shows a toughness fracture nature, resulting in superior ductility.

IV. CONCLUSIONS

In the present work, the effects of mechanical vibration and wall thickness on the microstructure and mechanical properties of AZ91D magnesium alloy produced by the expendable pattern shell casting process were investigated. The obtained results can be summarized in the following.

1. With the increase of wall thickness, the morphologies in α-Mg primary phase and β-$Mg_{17}Al_{12}$ phase obtained without vibration evolved from a fine dendrite to a coarse dendrite and from a fine continuous network structure to a coarse continuous network structure, respectively. With the application of mechanical vibration, the coarser dendrites transformed into fine and uniform equiaxed grains, and the previous coarse continuous network structure of β-$Mg_{17}Al_{12}$ phase changed to a discontinuous granular structure. The grain refinement degree increased with increasing vibration frequency and wall thickness.
2. The mechanical properties and density of AZ91D magnesium alloy without vibration continuously decreased with increasing wall thickness. The mechanical vibration greatly increased the mechanical properties and density of AZ91D magnesium alloy, particularly the larger wall thickness. The tensile strength, yield strength, elongation, and hardness of the sample with a wall thickness of 40 mm were, respectively, 60, 38, 58, and 59 pct higher than that of the sample without vibration.
3. The fractographs of the AZ91D magnesium alloy tensile samples without vibration revealed brittle fracture natures, while the fractographs of the AZ91D magnesium alloy tensile samples obtained with vibration showed toughness fracture natures, resulting in a superior ductility compared to that of the sample without vibration.

ACKNOWLEDGMENTS

This work was funded by Project 51204124 supported by the National Natural Science Foundation of China, Project P2015-09 supported by State Key Laboratory of Materials Processing and Die & Mould Technology, HUST, Project 2012M511610 & 2014T70694 supported by the China Postdoctoral Science Foundation, and Project K201415 supported by the Scientific Research Foundation of Wuhan Institute of Technology. The authors would also like to express their appreciation to the Analytical and Testing Center, HUST.

REFERENCES

1. Z.M. Li, Q.G. Wang, A.A. Luo, P.H. Fu, L.M. Peng, Y.X. Wu, and G.H. Wang: *Metall. Mater. Trans. A*, 2013, vol. 44A, pp. 5202–15.
2. D.R. Ni, D.L. Chen, J. Yang, and Z.Y. Ma: *Mater. Des.*, 2014, vol. 56, pp. 1–8.
3. B.L. Yu and J.Y. Uan: *Metall. Mater. Trans. A*, 2005, vol. 36A, pp. 2245–52.
4. H.A. Patel, D.L. Chen, S.D. Bhole, and K. Sadayappan: *J. Alloys Compd.*, 2010, vol. 496, pp. 140–48.
5. W.M. Jiang, Z.T. Fan, D.J. Liu, D.F. Liao, X.P. Dong, and X.M. Zong: *Mater. Sci. Eng. A*, 2013, vol. 560, pp. 396–403.
6. W.M. Jiang, Z.T. Fan, and D.J. Liu: *Trans. Nonferrous Met. Soc. China*, 2012, vol. 22, pp. 7–13.
7. D.F. Liao, Z.T. Fan, W.M. Jiang, E.Q. Shen, and D.J. Liu: *J. Mater. Process. Technol.*, 2011, vol. 211, pp. 1465–70.
8. M.C. Ashton, S.G. Sharman, and A.J. Brookes: *Mater. Des.*, 1984, vol. 5, pp. 66–67.
9. W.M. Jiang, Z.T. Fan, D.F. Liao, X.P. Dong, and Z. Zhao: *Int. J. Adv. Manuf. Technol.*, 2010, vol. 51, pp. 25–34.
10. S. Candan, M. Unal, M. Turkmen, E. Koc, Y. Turen, and E. Candan: *Mater. Sci. Eng. A*, 2009, vol. 501, pp. 115–18.
11. H. Yu, S.N. Chen, W. Yang, Y.L. Zhang, and S.H. Chen: *J. Alloys Compd.*, 2014, vol. 589, pp. 479–84.
12. M.J. Li, T. Tamura, N. Omura, and K. Miwa: *J. Alloys Compd.*, 2009, vol. 487, pp. 187–93.
13. M.J. Li, T. Tamura, and K. Miwa: *J. Mater. Res.*, 2007, vol. 22, pp. 3465–74.
14. A.M. Khosro and B. Niroumand: *J. Alloys Compd.*, 2011, vol. 509, pp. 114–22.
15. X.B. Liu, Y. Osawa, S. Takamori, and T. Mukai: *Mater. Sci. Eng. A*, 2008, vol. 487, pp. 120–23.
16. Z.W. Shao, Q.C. Le, Z.Q. Zhang, and J.Z. Cui: *Mater. Des.*, 2011, vol. 32, pp. 4216–24.
17. G. Chirita, I. Stefanescu, D. Soares, and F.S. Silva: *Mater. Des.*, 2009, vol. 30, pp. 1575–80.
18. A.F. Olufemi and I.S. Ademola: *Int. J. Metall. Eng.*, 2012, vol. 1, pp. 40–43.
19. F. Taghavi, H. Saghafian, and Y.H.K. Kharrazi: *Mater. Des.*, 2009, vol. 30, pp. 1604–11.
20. H.M. Guo, A.S. Zhang, X.J. Yang, M.M. Yan, and Y. Ding: *Metall. Mater. Trans. A*, 2014, vol. 45A, pp. 438–46.

21. S.L. Lü, S.S. Wu, L. Wan, and P. An: *Metall. Mater. Trans. A*, 2013, vol. 44A, pp. 2735–45.
22. W.M. Jiang, Z.T. Fan, Y.C. Dai, and C. Li: *Mater. Sci. Eng., A*, 2014, vol. 597, pp. 237–44.
23. J. Campbell: *Int. Mater. Rev.*, 1981, vol. 2, pp. 71–106.
24. R.D. Doherty: *Scripta Mater.*, 2003, vol. 49, pp. 1219–22.
25. F. Taghavi, H. Saghafian, and Y.H.K. Kharrazi: *Mater. Des.*, 2009, vol. 30, pp. 115–21.
26. N. Abu-Dheir, M. Khraisheh, K. Saito, and A. Male: *Mater. Sci. Eng., A*, 2005, vol. 393, pp. 109–17.
27. S. Lun Sin, D. Dubé, and R. Tremblay: *Mater. Charact.*, 2008, vol. 59, pp. 178–87.
28. G.E. Dieter: *Mechanical Metallurgy*, McGraw-Hill Book Co., New York, 1961, pp. 121–22.
29. K.B. Nie, X.J. Wang, K. Wu, M.Y. Zheng, and X.S. Hu: *Mater. Sci. Eng., A*, 2011, vol. 528, pp. 7484–87.
30. Z.F. Li, J. Dong, X.Q. Zeng, C. Lu, and W.J. Ding: *Mater. Sci. Eng. A*, 2007, vol. 466, pp. 134–39.
31. T.J. Chen, L.K. Huang, X.F. Huang, Y. Ma, and Y. Hao: *J. Alloys Compd.*, 2013, vol. 556, pp. 167–77.